Available online at www.sciencedirect.com
ScienceDirect
Trans. Nonferrous Met. Soc. China 34(2024) 2552−2562
Transactions of Nonferrous Metals Society of China
www.tnmsc.cn

In-situ Micro-CT analysis of deformation behavior in sandwich-structured meta-stable beta Ti−35Nb alloy

Yu-jing LIU[1], Zi-lin ZHANG[1], Jin-cheng WANG[2],
Xiang WU[1], Xiao-chun LIU[1], Wei-ying HUANG[3], Lai-chang ZHANG[2]

1. Institute of Metals, School of Materials Science and Engineering,
Changsha University of Science & Technology, Changsha 410004, China;
2. Centre for Advanced Materials and Manufacturing, School of Engineering,
Edith Cowan University, Joondalup, Perth, WA 6027, Australia;
3. College of Energy and Power Engineering, Changsha University of Science & Technology, Changsha 410004, China

Received 11 January 2023; accepted 4 October 2023

Abstract: Beta Ti−35Nb sandwich-structured composites with various reinforcing layers were designed and produced using additive manufacturing (AM) to achieve a balance between light weight and high strength. The impact of reinforcing layers on the compressive deformation behavior of porous composites was investigated through micro-computed tomography (Micro-CT) and finite element method (FEM) analyses. The results indicate that the addition of reinforcement layers to sandwich structures can significantly enhance the compressive yield strength and energy absorption capacity of porous metal structures; Micro-CT in-situ observation shows that the strain of the porous structure without the reinforcing layer is concentrated in the middle region, while the strain of the porous structure with the reinforcing layer is uniformly distributed; FEM analysis reveals that the reinforcing layers can alter stress distribution and reduce stress concentration, thereby promoting uniform deformation of the porous structure. The addition of reinforcing layer increases the compressive yield strength of sandwich-structured composite materials by 124% under the condition of limited reduction of porosity, and the yield strength increases from 4.6 to 10.3 MPa.

Key words: beta titanium alloy; sandwich-structured composite; in-situ micro-computed tomography; finite element modeling; compressive behavior

1 Introduction

Commercially pure titanium (CP-Ti) and Ti−6Al−4V alloys have been widely developed for biomedical and bone implant applications because of their excellent strength-to-modulus ratio, high biocompatibility, and superior corrosion resistance [1−3]. Nevertheless, both CP-Ti and Ti−6Al−4V still have a higher elastic modulus (~110 GPa) than β-type titanium alloys (50−90 GPa) [4−8]. A relatively low elastic modulus is significantly important to relieve the stress shielding effect caused by the difference in elastic modulus between the surgical implant and nature bone, thereby minimizing natural bone resorption and preventing implant premature failure [9]. The cytotoxic elements of Al and V in Ti−6Al−4V can cause adverse reactions with body fluids and tissues, leading to neurological disorders and diseases [10], which makes the Ti−6Al−4V not an ideal biomaterial to be used over a long period in the human body. By contrast, the elements Nb, Ta, and Mo are non-toxic, non-allergenic, and excellent β phase stabilizers in titanium alloys [11−13]. Compared to Mo and Ta, the lower density of Nb

Corresponding author: Wei-ying HUANG, E-mail: huangwy@csust.edu.cn; Lai-chang ZHANG, E-mail: l.zhang@ecu.edu.au
DOI: 10.1016/S1003-6326(24)66559-3

has the advantage to make lighter components. In addition, the *β*-type titanium alloys play an important role in optimizing performance of orthopedic implants by combining high ductility with appropriate corrosion resistance [14,15]. Thus, the *β*-type Ti−Nb−Ta−Zr [15,16] and Ti−Nb−Zr−Mo−Sn [17,18] alloys have been developed and studied to satisfy the biomedical requirements. Yet, the developed *β*-type titanium alloys still exhibit higher elastic modulus than the human bones.

The fabrication of porous metallic biomaterials using additive manufacturing (AM) techniques has been attracting considerable attention in recent years. AM can precisely fabricate titanium-based parts and scaffolds with customized porosity and complex structure that normally cannot be realized by conventional manufacturing methods. The porous structures with lower elastic modulus can facilitate the bone cells and tissues in-growth [19]. The mechanical behavior of porous structure has shown promising trends in the application of AM for biomedical bone implants [20,21]. The enhanced biological fixation through bones and interconnected pores has advanced bone tissue engineering applications [22,23]. One of its main advantages is that AM can obtain load-optimized structures and bionic implants that are not achievable through conventional techniques like sintering, casting, forging, or machining [24−27]. For example, AM provides an innovative solution for manufacturing near-shape metal parts with complex geometries, such as inter-connected porous scaffold and structure, which allows the bone tissues to growth and improve the fixation [27−31]. As aforementioned, the metastable *β*-Ti alloys enable implant made of them to have closer elastic modulus to that of human bones, offering an effective approach to minimize the stress shielding effect. Furthermore, due to promising superelasticity, metastable *β*-type titanium porous alloys have also been widely explored for shape memory and energy damping applications [16,32]. Researches in the design and manufacture of titanium porous structures, such as diamond cells [33], gyroid scaffolds [1], rhombic dodecahedron, and cubic structures [34] as well as gradient cellular structures [2], have attracted extensive attention. It has been reported that the rhombic dodecahedron and graded structures possess high-energy absorption [2,34,35]. Recently, the metastable *β*-type binary Ti−Nb alloys have become popular due to their excellent balance of strength and ductility, superb corrosion resistance [3,36−38] as well as the relatively low elastic modulus [17,39] and high biocompatibility [40,41] in the human body [42,43]. In particular, Ti−Nb alloys have shown lower elastic modulus, better apatite-forming capability, and cell proliferation compared to the CP-Ti [44−46]. The implant components produced by AM usually contain porous structure, which can reduce elastic modulus greatly and promote the growth of osteoblasts [47]. The rhombic dodecahedron porous structure is one of the commonly used structures in human implant. However, the strength of the rhombic dodecahedron porous structure is still low as a structure material. The sandwich structure can enhance the strength without changing the porous unit cell. The sandwich structure is light in weight, high in specific strength, and large in specific stiffness, so the deformation of the sandwich structure is small when subjected to external forces [48]. In addition, the sandwich structure has high natural frequency, good anti-fatigue properties, as well as excellent thermal insulation function and sound insulation and noise reduction [49]. Thus, the investigation on the mechanical properties and deformation mechanism of sandwich composite porous structures can offer alternative solutions for improving the compressive strength.

In this work, Ti−35Nb sandwich-structured composites (with rhombic dodecahedron unit cell) were fabricated by AM. The mechanical behavior was evaluated using compression tests. The deformation mechanisms were studied using micro-computed tomography (Micro-CT) system and finite element method (FEM). The experimental results combined with the FEM analysis provide significant insight into the deformation behavior and the strengthening mechanism of the sandwich-structured composites.

2 Experimental

The prealloyed Ti−35Nb powder (with particle size of 45−75 μm) was gas atomized from an alloyed ingot with analyzed chemical composition of 34.12 Nb, 0.10 O, and balance Ti (wt.%). The porous samples were built on a Ti substrate plate (preheated to 200 °C) with a selective laser melting

(SLM) machine. The preheated substrate plate can lower the temperature difference (thermal strain) between the solidified layers and molten pools, which in turn, can reduce the residual stress and mitigate solidification cracking. During the AM fabrication process, the build chamber was filled with Ar to reduce the oxygen content to <0.1 vol.% (minimize oxidation) and maintain the chamber pressure at ~1.03 kPa. The energy density (E, in J/mm^3) could be calculated via Eq. (1), which is a function of the processing parameters that can quantify the values of the processing parameters to tailor the microstructure, reduce the defects, and enhance the mechanical properties of porous structures [50]:

$$E=\frac{P}{vst} \tag{1}$$

where P is the laser power (W), v is the laser scan speed (mm/s), s is the hatch spacing (mm), and t is the single powder layer thickness (mm). The optimized processing parameters for porous Ti−35Nb alloy suggested that 53 J/mm^3 was an optimized energy density under the combination of P=200 W, s=0.1 mm, v=750 mm/s, and t=0.05 mm. The alternating scanning strategy with the scanning vector rotated by 90° was employed to reduce the residual stress due to the localized heating and rapid cooling, thereby strengthening the bonding between neighboring tracks and layers. Designed sandwich composite consisted of rhombic dodecahedron unit cells. The 3D CAD models were created by the Magic software. The single unit size of the porous structure is 3.5 mm × 3.5 mm × 3.5 mm, and the whole sample size was 14 mm (height) × 7 mm (width) × 7 mm (length). Figure 1(a) shows the rhombic dodecahedron structure (0L) with a porosity of 80%. Figure 1(b) shows the sandwich composite (78% porosity) with 1 reinforcing layer (1L) in the middle of the structure. The sandwich composite with 3 reinforcing layers (3L) in Fig. 1(c) had a porosity of 76%.

The specimens were compressed using an Instron 5982-universal machine at a constant strain rate of 0.5 mm/min at ambient temperature. Testing was stopped after the strain reached 3%, 6%, 9%, 12%, and 18%. The morphologies (at different plastic strains) of the samples tested in compression were then characterized by the Micro-CT. The

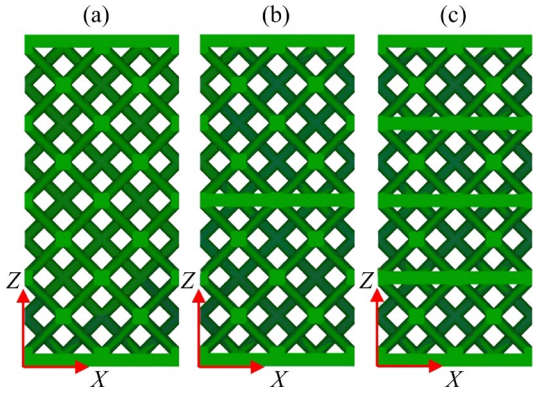

Fig. 1 3D CAD model of sandwich-structured composite with reinforcing layers and porous structure unit cell of rhombic dodecahedron: (a) 0 layer (0L); (b) 1 reinforcing layer (1L); (c) 3 reinforcing layers (3L)

tomographic scanning was conducted under 120 kV and 10 W with an exposure time of 2 s, using a voxel size of 6 μm and 3201 projections. Finite element modeling (FEM) was conducted by using Abaqus 2020 software. Samples for microstructure characterization were ground by using silicon carbide papers up to 2000 grits. The ground samples were then ultrasonically cleaned in distilled water for 10 min, and sequentially polished with MD-Mol and MD-Chem polishing clothes by following the standard metallographic procedures. The Kroll's reagent (5 vol.% hydrofluoric acid, 10 vol.% nitric acid, and 85 vol.% water) was used to further etch the surface of prepared specimens to analyze the morphology of struts. The constituent phase of the built samples was examined from the XY-plane (scanning plane) by X-ray diffraction (XRD, PANalytical Empyrean, Netherlands) with Cu K_α radiation (wavelength λ=0.15406 nm) at 40 kV and 40 mA. A step size of 0.013° and a scanning rate of 0.02 (°)/s were used to scan in the range from 30° to 80° (scanning angle (2θ)). The scanning electron microscope (SEM, FEI Verios XHR 460) [34] was used to characterize the microstructure and phases.

3 Results and discussion

3.1 Microstructure of composite

The morphology of gas-atomized prealloyed Ti−35Nb powder with a standard spherical shape, various sizes and smooth surface finish is shown in Fig. 2(a). Spherical powder particle morphology

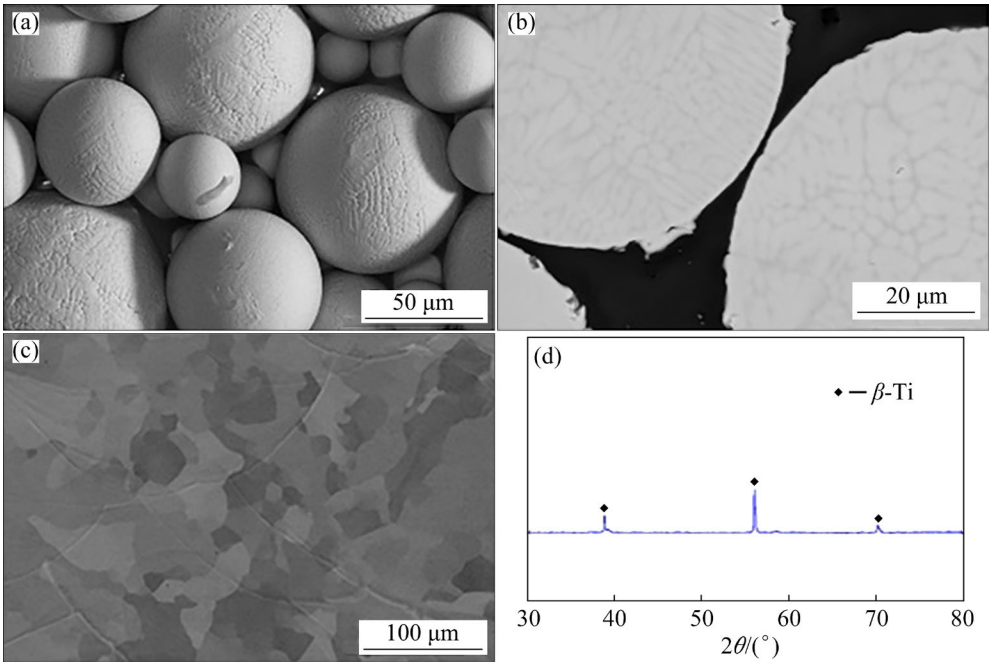

Fig. 2 SEM images showing morphology for powder (a), cross section (b), and sandwich-structured composite (c); XRD pattern of Ti−35Nb sandwich-structured composite (d)

can enhance the powder flowability, resulting in lower friction and improved powder apparent density (packing density). These are beneficial to printability when compared to irregularly shaped powders [4]. The cross section of the powder particle (Fig. 2(b)) indicates an equiaxial dendritic and homogeneous microstructure, where no micro-segregation is observed. This observation indicates the absence of compositional variations within the particle. Figure 2(c) shows the backscattered electron images in the scanning plane for the AM-fabricated Ti−35Nb alloy. There is no segregation or undissolved Nb particles, suggesting that a homogeneous microstructure is achieved. Figure 2(d) shows the XRD pattern for a single β phase for AM-fabricated Ti−35Nb alloy.

3.2 Mechanical behavior of sandwich-structured composites

In general, there are some deviations between the AM-produced sample and the designed model, which is generally attributed to the processing input energy. Usually, the porosity of the porous sample is analyzed from Micro-CT data. The Micro-CT images of the AM-produced sandwich-structured composite are shown in Fig. 3. The rhombic dodecahedron porous structure and the reinforcing layers are well manufactured without defect and

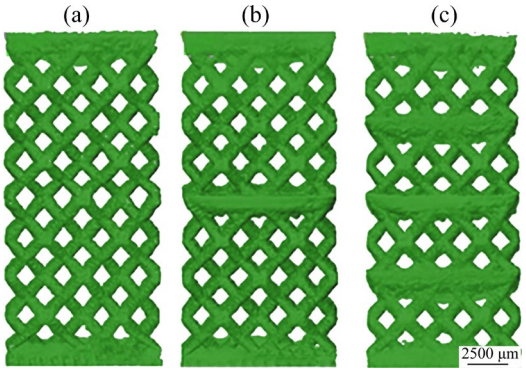

Fig. 3 Micro-CT images of sandwich-structured composite with reinforcing layers and porous structure unit cell of rhombic dodecahedron: (a) 0 layer (0L); (b) 1 reinforcing layer (1L); (c) 3 reinforcing layers (3L)

crack. The thickness of the reinforcing layers is ~1 mm. The porosities of the three composites are obtained from Micro-CT data: 80% (0L), 76% (1L) and 72% (3L) respectively. The engineering compressive stress−strain curves of sandwich-structured composites with different reinforcing layers are shown in Fig. 4. It can be seen that all the compressive curves present three deformation stages, i.e., the initial linear elastic deformation stage, the plateau plastic deformation stage, and the densification process stage (sharp increase in stress). The specimen without layer (0L) has the lowest compressive strength but the largest ductility (long

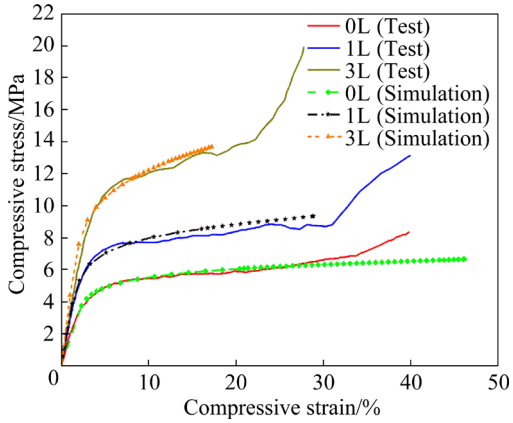

Fig. 4 Engineering compressive stress−strain curves of AM-manufactured sandwich-structured composites with different layers and corresponding curves from simulated models

plateau plastic deformation region). By contrast, the sample with one reinforcing lay (1L) shows a significant increase in compressive strength but a slight decrease in ductility. The curve of the sample with three layers (3L) shows a further increase in compressive yield strength but a large decrease in plastic strain. The compression yield strength of sandwich-structured composites with reinforcing layers (~10.3 MPa) is more than two times that of the porous structure without reinforcing layer (~4.6 MPa). In addition, the stress−strain curves from the experimental results are in a good agreement with those from the simulated results, indicating high accuracy of the FEM results.

The addition of the reinforcing layer brings about great changes in the deformation process of porous structure. Figure 5(a) shows that the rhombic dodecahedron structure without the reinforcing layer (0 layer) deforms gradually via increasing compressive strain from 3% to 18%. At the strain of 18%, it is apparent that the large shape deformation occurs at the center of the specimen (highlighted by a light blue color). By contrast, the rhombic dodecahedron structure with one layer (1L) in Fig. 5(b) shows that the deformation occurs

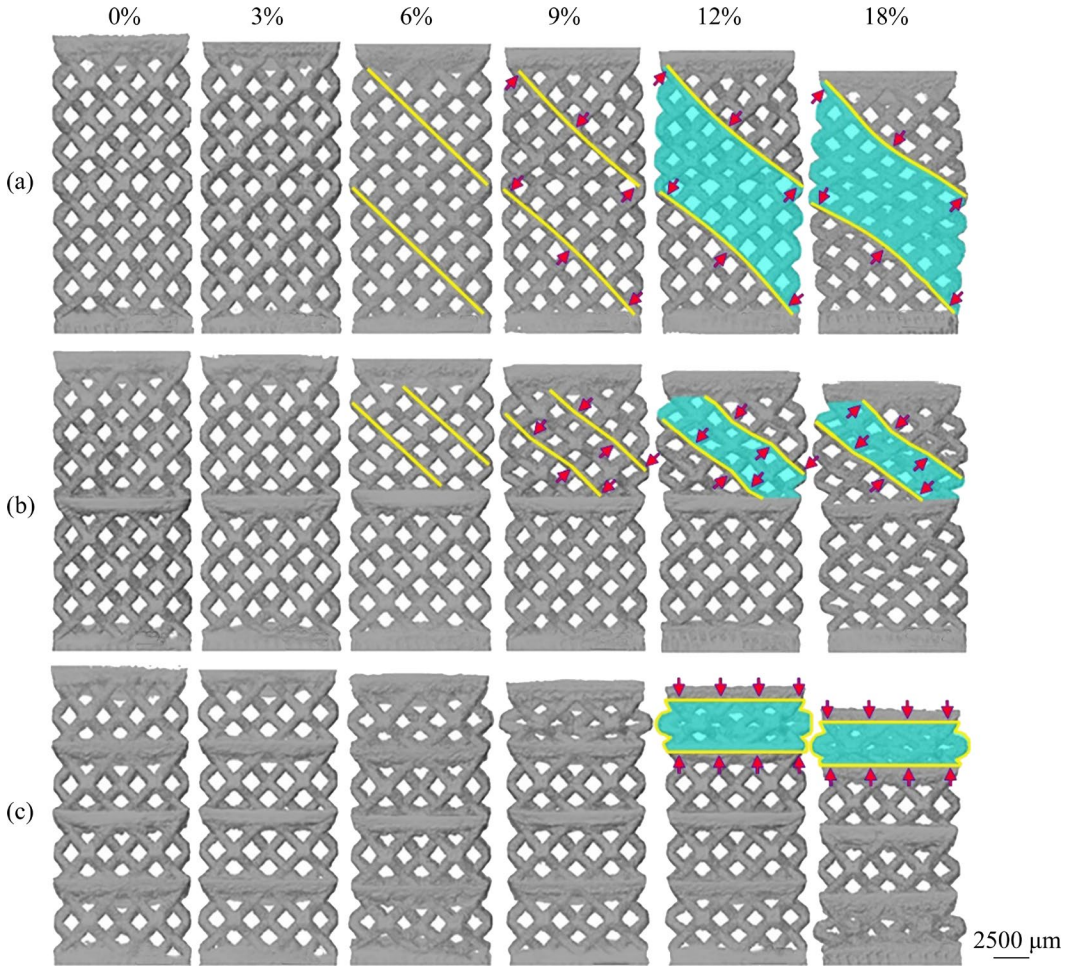

Fig. 5 In-situ Micro-CT images of AM-manufactured Ti−35Nb sandwich composite with rhombic dodecahedron unit cell at different strains during compression: (a) 0 layer (0L); (b) 1 layer (1L); (c) 3 layers (3L)

on the upper section. At the strain of 18%, the shape deformation mainly concentrates on the top region, whereas the area below the layer does not undergo significant distortion. Interestingly, Fig. 5(c) shows unique compressive deformation behavior for the sandwich composite with three layers (3L) when increasing the strain from 3% to 18%. At the strain of 12%, the evident deformation in shape can only be spotted above the top layer (as marked by a light blue color). While increasing the strain to 18%, the bottom section below the last layer then undergoes severe plastic deformation, whereas the porous regions in the middle of composite experiences limited deformation. The results reveal that the addition of reinforcing layers in the porous structure can exert a significant influence on the deformation during compression loading process.

It is known that the compression of porous structural materials is a complex process. The compression yield strength of the porous sample is mainly determined by the unit cell structure. Theoretically, the stress loaded on the porous structure can be decomposed into bending stress and buckling stress, which are affected by the geometry of the unit cell. However, the factors such as irregularities of the struts and the effect of internal microstructure need to be further considered to obtain accurate numerical analysis. The cumulative effect of both bending and buckling on the struts can largely affect the mechanical properties of the porous structure under the compression loads [51]. The optimization of unit cell and structure can improve the bending and buckling behavior to enhance the strength and ductility. The detailed simulation results can be used to analyze the local stress analysis and the deformation behavior of struts [52]. For a porous structure, the stress concentration area is usually on the node in the center area of the porous structure, where the beta titanium yields at the early stage of compression. This has been verified by the FEM results shown in Fig. 6. As the compression progresses, the yield of beta titanium would lead to the change of local structure in terms of the angle

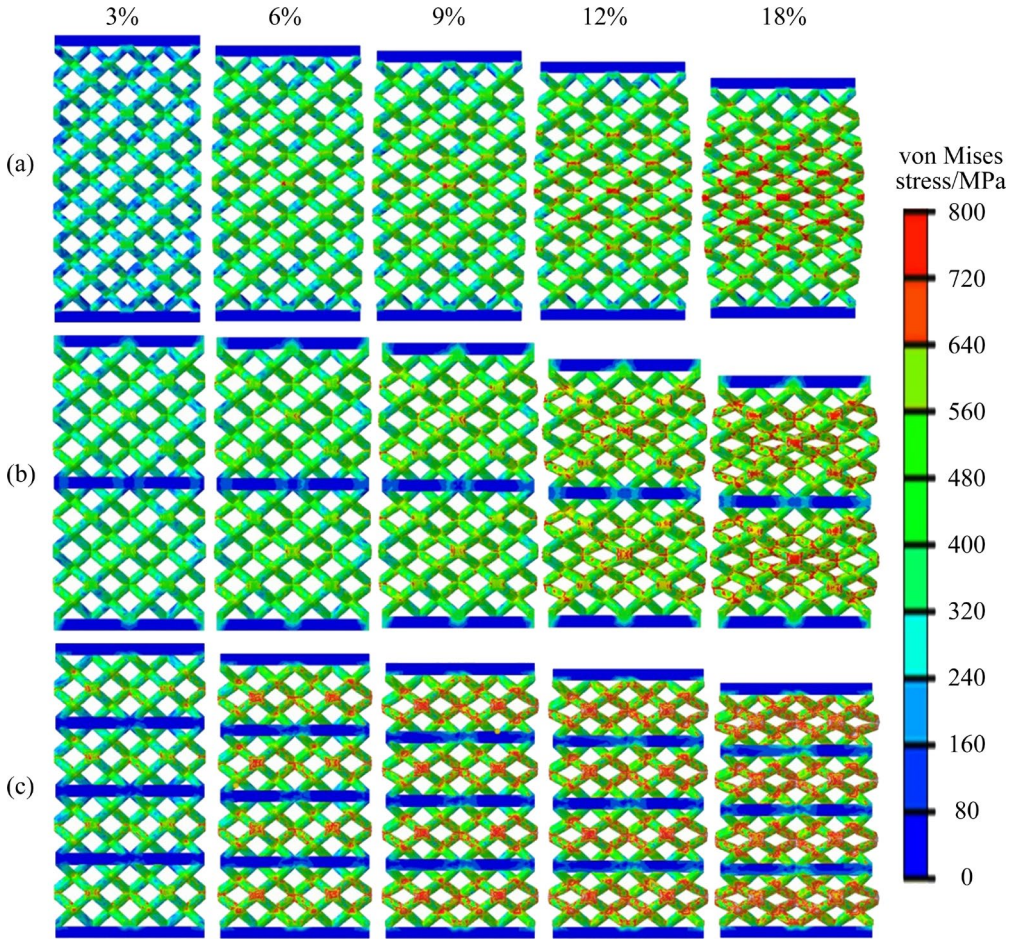

Fig. 6 Finite element analysis of sandwich composites with rhombic dodecahedron unit cell at different strains during compression: (a) 0 layer (0L); (b) 1 layer (1L); (c) 3 layers (3L)

between struts (Fig. 6(a)). Subsequently, as the compression continues, the angles of the struts at the nodes undergo further changes (Figs. 6(b, c)), impacting the stress distribution and ultimately leading to the overall macroscopic yield of the structure. As such, to ensure an accurate numerical analysis of the porous metallic composites, a comprehensive consideration of factors such as irregularities in the struts and the influence of the internal microstructure is essential. These factors play a significant role in shaping the mechanical behavior of the composites and need to be carefully accounted for in computational models.

3.3 Deformation mechanism of sandwich-structured composites

The strength of the porous samples can be tailored by changing the angle between the struts. Previous study [53] reported that the mechanical properties could be improved by varying the geometry of porous structures, mainly through changing the bending stress and buckling stress to alter the stress concentration. Figure 7(d) shows that the external compressive load p can be decomposed into component force p_1 (bending deformation) and p_2 (buckling deformation). The magnitude of forces p_1 and p_2 is directly related to the strut angle θ and external load p. The angle variation has an important influence on the mechanical properties of rhombic dodecahedron structure. The decrease in θ can lead to an increase in the bending force p_1, resulting in enhanced ductility and reduced strength. As such, the structure design can prevent the porous cell from brittle deforming to balance the strength and ductility by optimizing the bending deformation mechanism. However, the macroscopic plastic deformation behavior is difficult to be controlled by changing the geometry of porous structures. The introduction of the reinforcing layer is necessary to overcome this shortage, which can constrain the bending strain and increasing the buckling strain at the center of the structure, thereby increasing the compressive strength of the composite. As shown in FEM results in Fig. 6, the addition of the reinforcing layer results in a more uniform stress distribution within the sample, greatly reducing the highly localized stress concentration during macroscopic plastic deformation. The simulation results demonstrate that the maximum stress appears at the center region of the rhombic dodecahedron structure, and the struts undergo the bending deformation under the tensile and compressive stress. This result agrees well with the Micro-CT analysis (Fig. 5). It is apparent that the maximum stress of the 0L group is concentrated on the connected cross nodes, which are the stress concentration regions and are marked by the red color (Fig. 7(a)). With the addition of the reinforcing layer in the structure, the stress distribution of the porous structure is changed. Specifically, the bending strain of the node in the center of the porous structure is restricted and the angle has limited change at 18% macro compression strain (Fig. 7(b)). The position of the stress concentration regions is transferred to the center between the reinforcing layers and the number is significantly increased correspondingly. The stress concentration regions in 3L group are evenly distributed at each node, which can improve the energy absorption and the yield strength greatly (Fig. 7(c)).

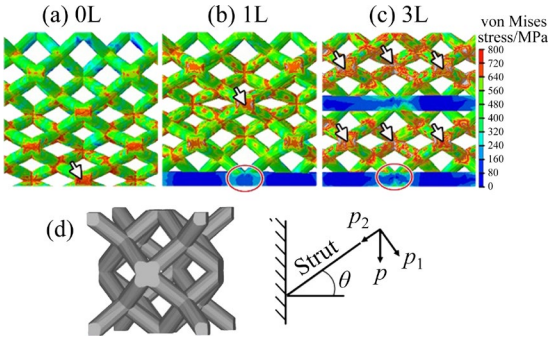

Fig. 7 Finite element analysis of sandwich composites with rhombic dodecahedron unit cell at 18% strain (a−c); Rhombic dodecahedron unit cell and schematic diagram showing applied load and corresponding bending and buckling vectors on strut (d)

In addition, the deformation process of the porous structure is changed by adding the reinforcing layers. In order to better understand this deformation process, a deformation model is built for the sandwich composite. In this work, the porous structure is a uniform lattice structure with a geometric symmetry, and the reinforcing layer is a solid material. The material of the porous structure is same as that of the reinforcing layer. When no force is applied, the neutral axis coincides with the geometric symmetry axis. When the force is applied, the neutral axis Z_p during plastic stage is

$$Z_p=\begin{cases}\dfrac{\lambda_\varepsilon z}{2},\ 0\le z<\dfrac{C(1-\varepsilon_{\mathrm{D}})}{2}\\ \dfrac{(C-\lambda_z-z)\varepsilon_{\mathrm{D}}}{2},\ \dfrac{C(1-\varepsilon_{\mathrm{D}})}{2}\le z\le C(1-\varepsilon_{\mathrm{D}})\end{cases}\tag{2}$$

The axial force N and bending moment M can be obtained from the neutral axis position:

$$N=\int_A\sigma\mathrm{d}A=\begin{cases}\sigma_{\mathrm{c}}bc+2\sigma_{\mathrm{f}}b(t-h),\ 0\le h<t\\ \sigma_{\mathrm{c}}b(c+2t)-2h,\ t\le h\le\dfrac{1}{2}(2t+c)\end{cases}\tag{3}$$

$$M=\int_A\sigma Z\mathrm{d}A=\begin{cases}\sigma_{\mathrm{f}}b(c+2t)^2\dfrac{h}{c+2t}\left(1-\dfrac{h}{c+2t}\right),\ 0\le h<t\\ \{\sigma_{\mathrm{f}}b[(c+2t)^2-c^2]+\\ \quad\sigma_{\mathrm{c}}b\left[c^2-((c+2t)^2)\left(1-2\dfrac{h}{c+2t}\right)^2\right]\}/4,\\ \quad t\le h\le\dfrac{1}{2}(2t+c)\end{cases}\tag{4}$$

where $\lambda_\varepsilon=\varepsilon_{\mathrm{D}}/(1-\varepsilon_{\mathrm{D}})$, C is the thickness of the lattice structure, ε_{D} is strain of the densification region in the lattice structure, σ_{f} is the yield strength of the reinforcing layer, σ_{c} is the yield strength of the lattice structure, b is the thickness of the lattice structure, t the thickness of the reinforcing layer, h is the distance from the neutral axis to reinforcing layer, and Z is the distance from geometric intermediate axis to plastic neutral axis. z is the thickness of the densified region, and during the loading process, $z=V_{\mathrm{c}}t_0$. V_{c} is strain rate of the reinforcing layer, V is the strain rate of the lattice structure, and $V_{\mathrm{c}}=(1-\varepsilon_{\mathrm{D}})V/\varepsilon_{\mathrm{D}}$. With the increase in time t_0, z also gradually increases, and the plastic neutral axis gradually moves closer to the reinforcing layer. When the core is fully densified, the plastic neutral axis coincides with the geometric symmetry axis. The yield criterion for sandwich composite has been derived, by taking into account of the non-uniformity of the lattice structure deformation. This criterion can be applied to both low-speed impact and static load conditions. The yield surface is symmetrical when the lattice structure is not compressed, but when it is partially densified, the yield surface becomes asymmetric. On the other hand, if the lattice structure is fully densified, the yield surface regains its symmetry. When the neutral axis is just at the interface between the densified region and the undeformed region, the plastic neutral axis Z_p reaches the maximum value, and the asymmetry of the yield materials reaches its maximum value.

4 Conclusions

(1) The compression tests show that the sandwich composites with different layers have different deformation behavior and mechanical properties.

(2) The addition of reinforcing layer increases the compressive yield strength of sandwich structure composite materials by 124%, and the yield strength increases from 4.6 to 10.3 MPa.

(3) The introduction of the reinforcing layer constrains bending strain and increases buckling strain at the center of the structure, thereby increasing the compressive strength of the composite.

(4) The stress concentration regions in 3L group are evenly distributed at each node, which can significantly improve the energy absorption and the yield strength greatly.

CRediT authorship contribution statement

Yu-jing LIU: Writing − Original draft, Investigation, Methodology, Funding acquisition, Writing − Review & editing; **Zi-lin ZHANG:** Investigation, Writing − Original draft, Writing − Review & editing, Data curation; **Jin-cheng WANG:** Writing − Original draft, Investigation, Validation, Formal analysis, Writing − Review & editing; **Xiang WU:** Writing − Review & editing; **Xiao-chun LIU:** Funding acquisition, Writing − Review & editing, Supervision; **Wei-ying HUANG:** Investigation, Writing − Review & editing; **Lai-chang ZHANG:** Investigation, Writing − Review & editing, Supervision.

Declaration of competing interest

The authors declare that they have no known competing financial interests or personal relationships that could have appeared to influence the work reported in this paper.

Acknowledgments

This research was supported by the Hunan Young Scientific Innovative Talents Program, China (No. 2020RC3040), Outstanding Youth Fund of Hunan Natural Science Foundation, China (Nos. 2021JJ20011,

2021JJ40600, 2021JJ40590), and the National Natural Science Foundation of China (Nos. 52001030, 52204371). Jin-cheng WANG is grateful for the support of the Forrest Research Foundation PhD Scholarship. The authors also acknowledge the facilities, and the scientific and technical assistance of the Australian Microscopy & Microanalysis Research Facility at the Centre for Microscopy, Characterisation & Analysis, The University of Western Australia, a facility funded by the University, State and Commonwealth Governments.

References

[1] WANG X H, LI J S, HU R, KOU H C, ZHOU L. Mechanical properties of porous titanium with different distributions of pore size [J]. Transactions of Nonferrous Metals Society of China, 2013, 23(8): 2317−2322.

[2] ZHAO S, LI S J, WANG S G, HOU W T, LI Y, ZHANG L C, HAO Y L, YANG R, MISRA R D K, MURR L E. Compressive and fatigue behavior of functionally graded Ti−6Al−4V meshes fabricated by electron beam melting [J]. Acta Materialia, 2018, 150: 1−15.

[3] ZHANG L C, CHEN L Y. A review on biomedical titanium alloys: recent progress and prospect [J]. Advanced Engineering Materials, 2019, 21: 1801215.

[4] SING S L, YEONG W Y, WIRIA F E. Selective laser melting of titanium alloy with 50 wt.% tantalum: Microstructure and mechanical properties [J]. Journal of Alloys and Compounds, 2016, 660: 461−470.

[5] LIU Y J, WANG H L, LI S J, WANG S G, WANG W J, HOU W T, HAO Y L, YANG R, ZHANG L C. Compressive and fatigue behavior of beta-type titanium porous structures fabricated by electron beam melting [J]. Acta Materialia, 2017, 126: 58−66.

[6] WANG J C, LIU Y J, RABADIA C D, LIANG S X, SERCOMBE T B, ZHANG L C. Microstructural homogeneity and mechanical behavior of a selective laser melted Ti−35Nb alloy produced from an elemental powder mixture [J]. Journal of Materials Science & Technology, 2021, 61: 221−233.

[7] LIU X C, LIU Z, LIU Y J, ZAFAR Z, LU Y J, WU X, JIANG Y, XU Z G, GUO Z H, LI S J. Achieving high strength and toughness by engineering 3D artificial nacre-like structures in Ti6Al4V−Ti metallic composite [J]. Composites Part B: Engineering, 2022, 230: 109552.

[8] LU Y J, LIU X C, LIU Y J, WU X, JIANG Y, LIU Z, LIN J X, ZHANG L C. Corrosion behavior of novel titanium-based composite with engineering 3D artificial nacre-like structures [J]. Composites Part A: Applied Science and Manufacturing, 2023, 164: 107278.

[9] NIINOMI M. Mechanical properties of biomedical titanium alloys [J]. Materials Science and Engineering A, 1998, 243: 231−236.

[10] NAG S, BANERJEE R, FRASER H L. Microstructural evolution and strengthening mechanisms in Ti−Nb−Zr−Ta, Ti−Mo−Zr−Fe and Ti−15Mo biocompatible alloys [J]. Materials Science and Engineering C, 2005, 25: 357−362.

[11] WENG W J, BIESIEKIERSKI A, LI Y C, WEN C. Effects of selected metallic and interstitial elements on the microstructure and mechanical properties of beta titanium alloys for orthopedic applications [J]. Materialia, 2019, 6: 100323.

[12] ZHURAVLEVA K, BÖNISCH M, PRASHANTH K G, HEMPEL U, HELTH A, GEMMING T, CALIN M, SCUDINO S, SCHULTZ L, ECKERT J, GEBERT A. production of porous β-type Ti−40Nb alloy for biomedical applications: Comparison of selective laser melting and hot pressing [J]. Materials (Basel, Switzerland), 2013, 6: 5700−5712.

[13] WANG J C, LIU Y J, QIN P, LIANG S X, SERCOMBE T B, ZHANG L C. Selective laser melting of Ti−35Nb composite from elemental powder mixture: Microstructure, mechanical behavior and corrosion behavior [J]. Materials Science and Engineering A, 2019, 760: 214−224.

[14] LIU Y J, LI S J, HOU W T, WANG S G, HAO Y L, YANG R, SERCOMBE T B, ZHANG L C. Electron beam melted beta-type Ti−24Nb−4Zr−8Sn porous structures with high strength-to-modulus ratio [J]. Journal of Materials Science & Technology, 2016, 32: 505−508.

[15] WANG J L, LIU R L, MAJUMDAR T, MANTRI S A, RAVI V A, BANERJEE R, BIRBILIS N. A closer look at the in vitro electrochemical characterisation of titanium alloys for biomedical applications using in-situ methods [J]. Acta Biomaterialia, 2017, 54: 469−478.

[16] HAFEEZ N, LIU J, WANG L Q, WEI D X, TANG Y J, LU W J, ZHANG L C. Superelastic response of low-modulus porous beta-type Ti−35Nb−2Ta−3Zr alloy fabricated by laser powder bed fusion [J]. Additive Manufacturing, 2020, 34: 101264.

[17] LIU Y J, ZHANG Y S, ZHANG L C. Transformation-induced plasticity and high strength in beta titanium alloy manufactured by selective laser melting [J]. Materialia, 2019, 6: 100299.

[18] JAWED S F, LIU Y J, WANG J C, RABADIA C D, WANG L Q, LI Y H, ZHANG X H, ZHANG L C. Tailoring deformation and superelastic behaviors of beta-type Ti−Nb−Mn−Sn alloys [J]. Journal of the Mechanical Behavior of Biomedical Materials, 2020, 110: 103867.

[19] LIANG H X, YANG Y W, XIE D Q, LI L, MAO N, WANG C J, TIAN Z J, JIANG Q, SHEN L D. Trabecular-like Ti−6Al−4V scaffolds for orthopedic: fabrication by selective laser melting and in vitro biocompatibility [J]. Journal of Materials Science & Technology, 2019, 35: 1284−1297.

[20] ZHANG L C, ATTAR H. Selective laser melting of titanium alloys and titanium matrix composites for biomedical applications: A review [J]. Advanced Engineering Materials, 2016, 18: 463−475.

[21] LIU Y J, LI X P, ZHANG L C, SERCOMBE T B. Processing and properties of topologically optimised biomedical Ti−24Nb−4Zr−8Sn scaffolds manufactured by selective laser melting [J]. Materials Science and Engineering A, 2015, 642: 268−278.

[22] WAUTHLE R, VAN D S J, YAVARI S A, VAN H J, KRUTH J P, ZADPOOR A A, WEINANS H, MULIER M, SCHROOTEN J. Additively manufactured porous tantalum implants [J]. Acta Biomaterialia, 2015, 14: 217−225.

[23] ZADPOOR A A, MALDA J. Additive manufacturing of biomaterials, tissues, and organs [J]. Annals of Biomedical Engineering, 2017, 45: 1−11.
[24] ABELE E, STOFFREGEN H A, KNIEPKAMP M, LANG S, HAMPE M. Selective laser melting for manufacturing of thin-walled porous elements [J]. Journal of Materials Science & Technology, 2015, 215: 114−122.
[25] HEDAYATI R, AHMADI S M, LIETAERT K, POURAN B, LI Y, WEINANS H, RANS C D, ZADPOOR A A. Isolated and modulated effects of topology and material type on the mechanical properties of additively manufactured porous biomaterials [J]. Journal of the Mechanical Behavior of Biomedical Materials, 2018, 79: 254−263.
[26] JOGUET D, COSTIL S, LIAO H, DANLOS Y. Porosity content control of CoCrMo and titanium parts by Taguchi method applied to selective laser melting process parameter [J]. Rapid Prototyping Journal, 2016, 22: 20−30.
[27] KARAJI Z G, SPEIRS M, DADBAKHSH S, KRUTH J P, WEINANS H, ZADPOOR A A, YAVARI S A. Additively manufactured and surface biofunctionalized porous nitinol [J]. ACS Applied Materials & Interfaces, 2017, 9: 1293−1304.
[28] PERRY C. Biomaterials — A tantalus experience [J]. Materials Today, 2011, 14: 230.
[29] ROTTA G, SERAMAK T, ZASINSKA K. Estimation of young's modulus of the porous titanium alloy with the use of fem package [J]. Advanced Materials Science, 2015, 15: 29−37.
[30] AMIN Y S, WAUTHLE R, VAN D S J, RIEMSLAG A C, JANSSEN M, MULIER M, KRUTH J P, SCHROOTEN J, WEINANS H, ZADPOOR A A. Fatigue behavior of porous biomaterials manufactured using selective laser melting [J]. Materials Science and Engineering C, 2013, 33: 4849−4858.
[31] MARKHOFF J, WIEDING J, WEISSMANN V, PASOLD J, JONITZ H A, BADER R. Influence of different three-dimensional open porous titanium scaffold designs on human osteoblasts behavior in static and dynamic cell investigations [J]. Materials, 2015, 8: 5490−5507.
[32] TALLING R J, DASHWOOD R J, JACKSON M, DYE D. On the mechanism of superelasticity in Gum metal [J]. Acta Materialia, 2009, 57: 1188−1198.
[33] VAN H B, APERS Y, LIETAERT K, KRUTH J P. Improving the fatigue performance of porous metallic biomaterials produced by selective laser melting [J]. Acta Biomater, 2017, 47: 193−202.
[34] LIU Y J, LI S J, ZHANG L C, HAO Y L, SERCOMBE T B. Early plastic deformation behaviour and energy absorption in porous β-type biomedical titanium produced by selective laser melting [J]. Scripta Materialia, 2018, 153: 99−103.
[35] LI S J, XU Q S, WANG Z, HOU W T, HAO Y L, YANG R, MURR L E. Influence of cell shape on mechanical properties of Ti−6Al−4V meshes fabricated by electron beam melting method [J]. Acta Biomater, 2014, 10: 4537−4547.
[36] DAI N W, ZHANG L C, ZHANG J X, CHEN Q M, WU M L. Corrosion behavior of selective laser melted Ti−6Al−4V alloy in NaCl solution [J]. Corrosion Science, 2016, 102: 484−489.
[37] CHEN Y, ZHANG J X, DAI N W, QIN P, ATTAR H, ZHANG L C. Corrosion behaviour of selective laser melted Ti−TiB biocomposite in simulated body fluid [J]. Electrochimica Acta, 2017, 232: 89−97.
[38] QIN P, LIU Y J, SERCOMBE T B, LI Y H, ZHANG C W, CAO C D, SUN H Q, ZHANG L C. Improved corrosion resistance on selective laser melting produced Ti−5Cu alloy after heat treatment [J]. ACS Biomaterials Science & Engineering, 2018, 4: 2633−2642.
[39] RACK H J, QAZI J I. Titanium alloys for biomedical applications [J]. Materials Science and Engineering C, 2006, 26: 1269−1277.
[40] CREMASCO A, MESSIAS A D, ESPOSITO A R, DUEK E A D R, CARAM R. Effects of alloying elements on the cytotoxic response of titanium alloys [J]. Materials Science and Engineering C, 2011, 31: 833−839.
[41] EISENBARTH E, VELTEN D, MÜLLER M, THULL R, BREME J. Biocompatibility of β-stabilizing elements of titanium alloys [J]. Biomaterials, 2004, 25: 5705−5713.
[42] BOSE S, KE D X, SAHASRABUDHE H, BANDYOPADHYAY A. Additive manufacturing of biomaterials [J]. Progress in Materials Science, 2018, 93: 45−111.
[43] ZHANG L C, CHEN L Y, WANG L Q. Surface modification of titanium and titanium alloys: Technologies, developments, and future interests [J]. Advanced Engineering Materials, 2020, 22: 1901258.
[44] ZHAO D L, HAN C J, LI J J, LIU J, WEI Q S. In situ fabrication of a titanium−niobium alloy with tailored microstructures, enhanced mechanical properties and biocompatibility by using selective laser melting [J]. Materials Science and Engineering C, 2020, 111: 110784.
[45] OLIVEIRA D C S S, GRIZA S, OLIVEIRA D M V, RIBEIRO A A, LEITE M B. Study of the porous Ti35Nb alloy processing parameters for implant applications [J]. Powder Technology, 2015, 281: 91−98.
[46] WANG J C, LIU Y J, LIANG S X, ZHANG Y S, WANG L Q, SERCOMBE T B, ZHANG L C. Comparison of microstructure and mechanical behavior of Ti−35Nb manufactured by laser powder bed fusion from elemental powder mixture and prealloyed powder [J]. Journal of Materials Science & Technology 2022, 105: 1−16.
[47] CHEN LY, LIANG S X, LIU Y J, ZHANG L C. Additive manufacturing of metallic lattice structures: Unconstrained design, accurate fabrication, fascinated performances, and challenges [J]. Materials Science and Engineering R: Reports, 2021, 146: 100648.
[48] RAMNATH B V, ALAGARRAJA K, ELANCHEZHIAN C. Review on sandwich composite and their applications [J]. Materials Today: Proceedings, 2019, 16: 859−864.
[49] LIN G J, LI J Q, LI F, CHEN P W, SUN W F. Low-velocity impact response of sandwich composite panels with shear thickening gel filled honeycomb cores [J]. Composites Communications, 2022, 32:110136.
[50] ATTAR H, BÖNISCH M, CALIN M, ZHANG L C, SCUDINO S, ECKERT J. Selective laser melting of in situ titanium–titanium boride composites: Processing, microstructure and mechanical properties [J]. Acta Materialia, 2014, 76: 13−22.
[51] ZHAO S, LI S J, HOU W T, HAO Y L, YANG R, MISRA R D K. The influence of cell morphology on the compressive

fatigue behavior of Ti−6Al−4V meshes fabricated by electron beam melting [J]. Journal of the Mechanical Behavior of Biomedical Materials, 2016, 59: 251−264.

[52] ZARGARIAN A, ESFAHANIAN M, KADKHODAPOUR J, ZIAEI-RAD S. Numerical simulation of the fatigue behavior of additive manufactured titanium porous lattice structures [J]. Materials Science and Engineering C, 2016, 60: 339−347.

[53] YAVARI S A, AHMADI S M, WAUTHLE R, POURAN B, SCHROOTEN J, WEINANS H, ZADPOOR A A. Relationship between unit cell type and porosity and the fatigue behavior of selective laser melted meta-biomaterials [J]. Journal of the Mechanical Behavior of Biomedical Materials, 2015, 43: 91−100.

三明治结构亚稳 β-Ti−35Nb 合金变形行为的原位 Micro-CT 分析

刘玉敬[1]，张自林[1]，王金成[2]，吴 翔[1]，刘小春[1]，黄伟颖[3]，张来昌[2]

1. 长沙理工大学 材料科学与工程学院 金属研究所，长沙 410004；
2. Centre for Advanced Materials and Manufacturing, School of Engineering, Edith Cowan University, Joondalup, Perth, WA 6027, Australia;
3. 长沙理工大学 能源与动力工程学院，长沙 410004

摘 要：利用增材制造(AM)技术制造具有不同增强层的 β 型 Ti−35Nb 合金三明治结构复合材料，以实现轻量化和高强度之间的平衡。通过原位微计算机断层扫描(Micro-CT)和有限元模拟法(FEM)研究增强层对多孔复合材料压缩变形行为的影响。结果表明，三明治结构加入增强层可显著提升多孔金属结构的压缩屈服强度和能量吸收能力；原位 Micro-CT 观察到未加入增强层的多孔结构应变集中在中间区域，而含有增强层多孔结构的应变则均匀分布；FEM 分析揭示加入的增强层会改变应力分布并降低应力集中，从而促进多孔结构整体均匀变形。在有限降低孔隙率的条件下，增强层的加入使三明治结构复合材料的压缩屈服强度提升 124%，屈服强度由 4.6 MPa 提升到 10.3 MPa。

关键词：β 钛合金；三明治结构复合材料；原位微计算机断层扫描；有限元模拟；压缩变形行为

(Edited by Bing YANG)